

Effect of Non-Newtonian Models on Blood Flow in Artery with Different Consecutive Stenosis

Mehdi Jahangiri*

Department of Mechanical Engineering,
Shahrekord Branch, Islamic Azad University, Shahrekord, Iran
E-mail: Jahangiri.M@iaushk.ac.ir

*Corresponding author

Ahmad Haghani

Department of Mechanical Engineering,
Shahrekord Branch, Islamic Azad University, Shahrekord, Iran
E-mail: A.Haghani@iaushk.ac.ir

Reza Ghaderi

Department of Mechanical Engineering,
Shahrekord Branch, Islamic Azad University, Shahrekord, Iran
E-mail: Reza.ghaderi@ymail.com

Seyyed Mohammad Hosseini Harat

Department of Mathematics,
Shahrekord Branch, Islamic Azad University, Shahrekord, Iran
E-mail: Smhosseini86@gmail.com

Received: 27 October 2017, Revised: 21 November 2017, Accepted: 20 December 2017

Abstract: In this paper, the ADINA finite element software was used for numerical investigation of laminar and non-Newtonian flow through a blood artery with consecutive stenosis. For modeling the non-Newtonian behavior of blood, six models were used, namely, Carreau, Carreau-Yasuda, modified Casson, Power law, generalized power law, and Walburn-Schneck. The results show that for all non-Newtonian models as well as the Newtonian model, the velocity of blood flow in the second stenosis is greater than the first stenosis. Also, up to 4D back of second stenosis, a reverse flow area is formed that causes the spread of disease and the formation of new plaque. As a general conclusion, it can be stated that due to the smaller values obtained from the power law and Walburn-Schneck models, as compared with the other models, for fluid velocity and wall shear stress, these two models must be applied with caution.

Keywords: ADINA, Endothelial cell, Reverse flow, Throat

Reference: Mehdi Jahangiri, Ahmad Haghani, Reza Ghaderi and Seyyed Mohammad Hosseini Harat, "Effect of Non-Newtonian Models on Blood Flow in Artery with Different Consecutive Stenosis", Int J of Advanced Design and Manufacturing Technology, Vol. 11/No. 1, 2018, pp. 79-86.

Biographical notes: **M. Jahangiri** is a faculty member of Technical & Engineering. His current research interest includes biomechanics and renewable energy. **A. Haghani** is a faculty member of Technical & Engineering. His current research focuses on composite materials and renewable energy. **R. Ghaderi** is a faculty member of Technical & Engineering. His current research focuses on nonlinear vibration. **S. M. Hosseini Harat** is a faculty member of science. His current research focuses on numerical and analytical solution of functional equations and numerical linear algebra.

1 INTRODUCTION

As blood flows through the stenosis, its non-Newtonian effects become more pronounced [1-4]. No model, Newtonian or otherwise, can comprehensively cover all the complicated characteristics of blood. For this reason, different models have to be used. The many differences existing among these models, Newtonian or otherwise, can lead to very different results [5-9]. Fry [10] stated that wall shear stresses greater than 40 Pa would damage the endothelial cells. Ramstack et al., [11] stated that a wall shear stress, greater than 100 Pa leads to endothelial cells damage and consequently, blood clots. In their investigation on the LDL particles mass transfer in the carotid artery, Fazli et al., [12] showed that a smaller reverse flow region is lead to more accumulation of LDL particles, which in turn increases plaque growth and

spreading. Investigation of velocity profiles leads to more accurate methods in the treatment of clogged arteries [12]. Investigation of shear stress on the wall for predicting damage in arteries is also essential [10], [11], [13-15].

With due regard to these facts, the present study aims to conduct an ADINA-aided analysis by using physiological pulses for investigating shear stress at artery walls, as well as the reverse flow region length inside a blood artery with consecutive stenosis. Since different non-Newtonian models exhibit different capabilities in describing various physical phenomena, the Newtonian as well as six non-Newtonian models were used in this study for simulating blood behaviour. The study of the effect of stenosis spacing on hemodynamic parameters such as blood velocity and wall shear stress of artery is a problem that has not been studied so far.

Table 1 Non-Newtonian models with given molecular viscosity of blood

$\mu = 0.0033$	Newtonian [8, 9, 13, 14]
$\mu = k \dot{\gamma} ^{n-1}, \quad k = 0.035, n = 0.6$	Power-law [17]
$\mu = \mu_{\infty} + (\mu_0 - \mu_{\infty}) (1 + A \dot{\gamma} ^2)^n$ $A = 10.976, n = -0.3216, \mu_{\infty} = 0.0033, \mu_0 = 0.056$	Carreau [17]
$\mu = \mu_i + \frac{\mu_0 - \mu_i}{[1 + (\lambda \dot{\gamma} ^b)]^a}$ $\mu_0 = 0.016, \mu_i = 0.0033, \lambda = 8.2, b = 1.23, a = 0.64$	Carreau-Yasuda [18]
$\mu = \left[\sqrt{\tau_y \left(\frac{1 - e^{-m \dot{\gamma} }}{ \dot{\gamma} } \right)} + \sqrt{\mu_c} \right]^2$ $\mu_c = 0.0033, m = 100$	Modified-Casson [19]
$\mu = k(\dot{\gamma}) \dot{\gamma} ^{n(\dot{\gamma})-1}$ $k(\dot{\gamma}) = \mu_{\infty} + \Delta\mu \exp \left[-\left(1 + \frac{ \dot{\gamma} }{a}\right) \exp\left(\frac{-b}{\dot{\gamma}}\right) \right]$ $n(\dot{\gamma}) = n_{\infty} - \Delta n \exp \left[-\left(1 + \frac{ \dot{\gamma} }{c}\right) \exp\left(\frac{-d}{\dot{\gamma}}\right) \right]$ $\mu_{\infty} = 0.0033, \Delta\mu = 0.25, n_{\infty} = 1, \Delta n = 0.45, a = 50, b = 3, c = 50, d = 4$	Generalized power law [20]
$\mu = a_1 \exp\left(a_2 + \frac{a_3}{H^2}\right) \dot{\gamma} ^{(1-a_4H)}$ $a_1 = 0.00797 \text{ Pa.s}, a_2 = 0.0608, a_3 = 377.7515, a_4 = 0.00499$	Walburn-Schneck [21]

2 GOVERNING EQUATION

The general form of the equations governing fluid motion, i.e., momentum and continuity equations, in ADINA are as follows [16]:

$$\frac{\partial(\rho V)}{\partial t} + \nabla \cdot (\rho V V - \bar{\tau}) = f_b \quad (1)$$

$$\frac{\partial \rho}{\partial t} + \nabla \cdot (\rho V) = 0 \quad (2)$$

Where t is time; ρ is density; V is velocity, f_b is volume vector force exerted on the fluid (assumed zero here), and $\bar{\tau}$ is stress tensor determined from the following equation:

$$\tau = -pI + 2\mu e \quad (3)$$

$$e = \frac{1}{2}(\nabla V + \nabla V^T) \quad (4)$$

In the above relation, p denotes pressure, I is the unit matrix, and μ is fluid viscosity. For modeling non-Newtonian fluid behavior, we used the models presented in Table 1.

3 PRESENT WORK

The blood artery model considered in the present study has symmetrical stenosis and rigid walls with stenosis percentages of 30, 50, and 70 percent. The equation for blood flow through the blood artery in the stenosis area is described as [22]:

$$\frac{R(z)}{R_0} = 1 - \left(\frac{R_0 - R_{0,t}}{2R_0} \right) \left(1 + \cos \frac{2\pi(z - z_m)}{L_{st}} \right) \quad (5)$$

Where R_0 is radius of the undamaged artery (equal to 0.015 m), $R(z)$ is blood artery radius at the stenosis area, $R_{0,t}$ is blood artery radius at the throat of the stenosis area, z_m is axial coordinate of the stenosis area, and L_{st} is length of the stenosis area. Moreover, lengths of the entrance region, the stenosis region, and the exit region are considered as $20R_0$, $4R_0$, and $42R_0$ respectively. As an incompressible non-Newtonian fluid, blood has a density of 1050 kg/m^3 and a viscosity of 0.0035 Pa.s . In this study, the right coronary artery pulse flow, presented by Zeng et al [23], was used (Fig. 1). Average flow rate of this pulse is 1.65 ml/s and cardiac cycle is 0.8 seconds. To obtain results that are independent of the grid, and to determine the best situation regarding accuracy of solutions and minimization of computer run time, a 30-node meshing was used across the artery [24].

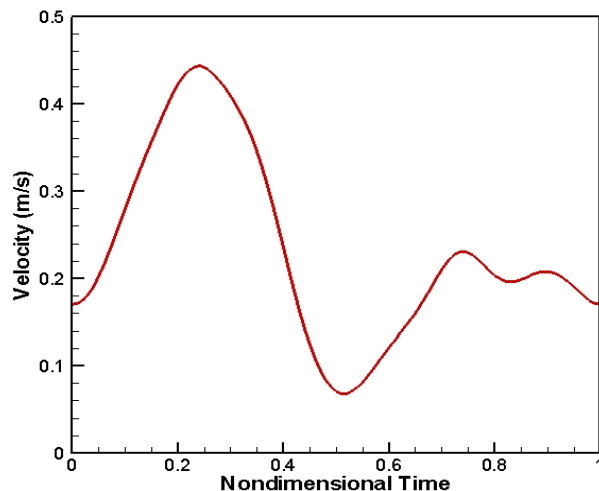


Fig. 1 Average inlet velocity profile [23]

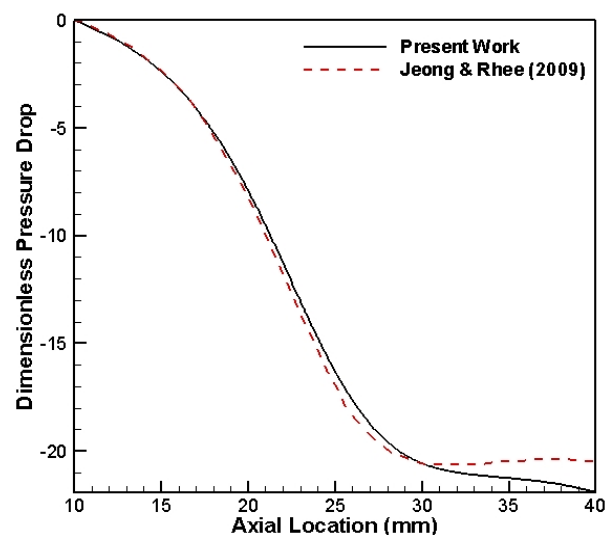


Fig. 2 Non-dimensional pressures in axial direction

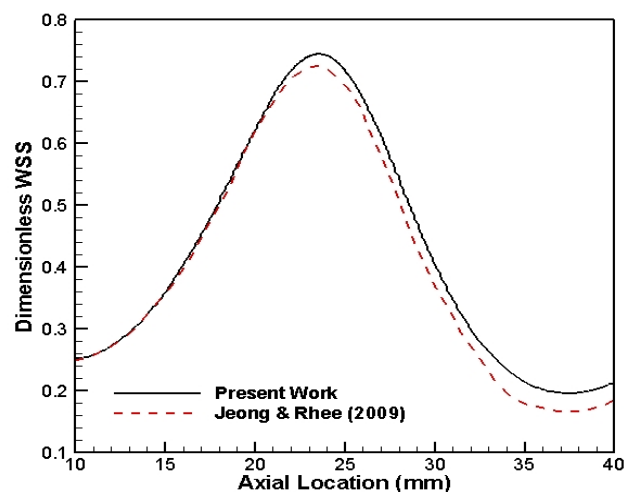


Fig. 3 Non-dimensional WSS in axial direction

4 RESULTS

To investigate the validity of the numerical solution used in the unsteady state in the presence of stenosis, the numerical method used by Jeong et al [25] was implemented. In Figs. 2 and 3, non-dimensional pressures and stresses obtained from this study are compared with those obtained by Jeong et al. As can be seen, these results are in very good agreement. Fig. 4 shows the locations of the 8 sections considered in this

study: Section 1 at a distance of 1 diameter before the first stenosis, Section 2 at the throat of the first stenosis area, Section 3 at a distance of 1 diameter after the first stenosis, Section 4 at a distance of 2 diameters after the first stenosis, Section 5 at a distance of 1 diameter before the second stenosis, Section 6 at the throat of the second stenosis area, Section 7 at a distance of 1 diameter after the throat of the second stenosis area, and Section 8 at a distance of 4 diameters after the throat of the second stenosis area.

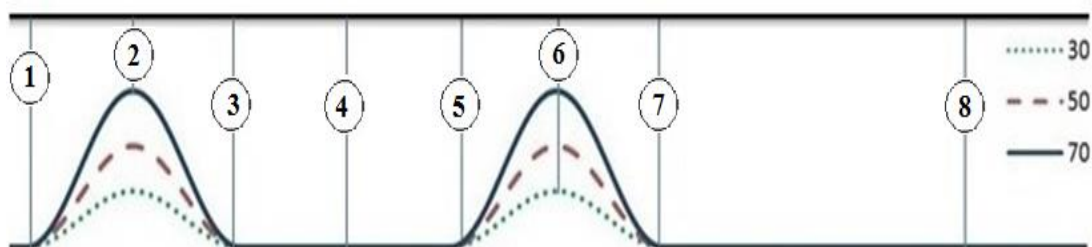
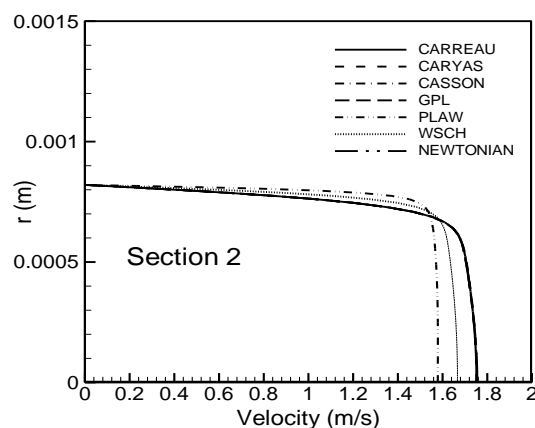
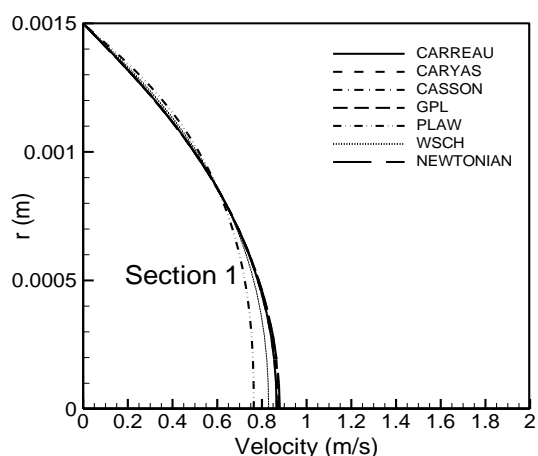


Fig. 4 Geometry of artery with stenosis, stenosis length=2D, distance between of two stenosis=4D

Fig. 5 shows the velocity profile at different sections at $t = 0.24$ s in artery with 70% stenosis for the Newtonian and the six non-Newtonian models. As can be seen in the figure 5, velocity values obtained from the Newtonian model as well as the Carreau, Carreau-Yasuda, Casson, and the generalized power law method are very close. Moreover, Fig. 5 shows that velocity at the throat of second stenosis is much more than throat of first

stenosis. The reason is that, after passing through the first stenosis, the flow is diverted towards the central axis of the artery. The value obtained for minimum velocity at section 6 (throat of the second stenosis area) is zero for all the models, and is equal to the velocity at the wall. This indicates that no reverse flow exists at this section. As expected, the maximum velocity occurred at section 6 (throat of the stenosis area).



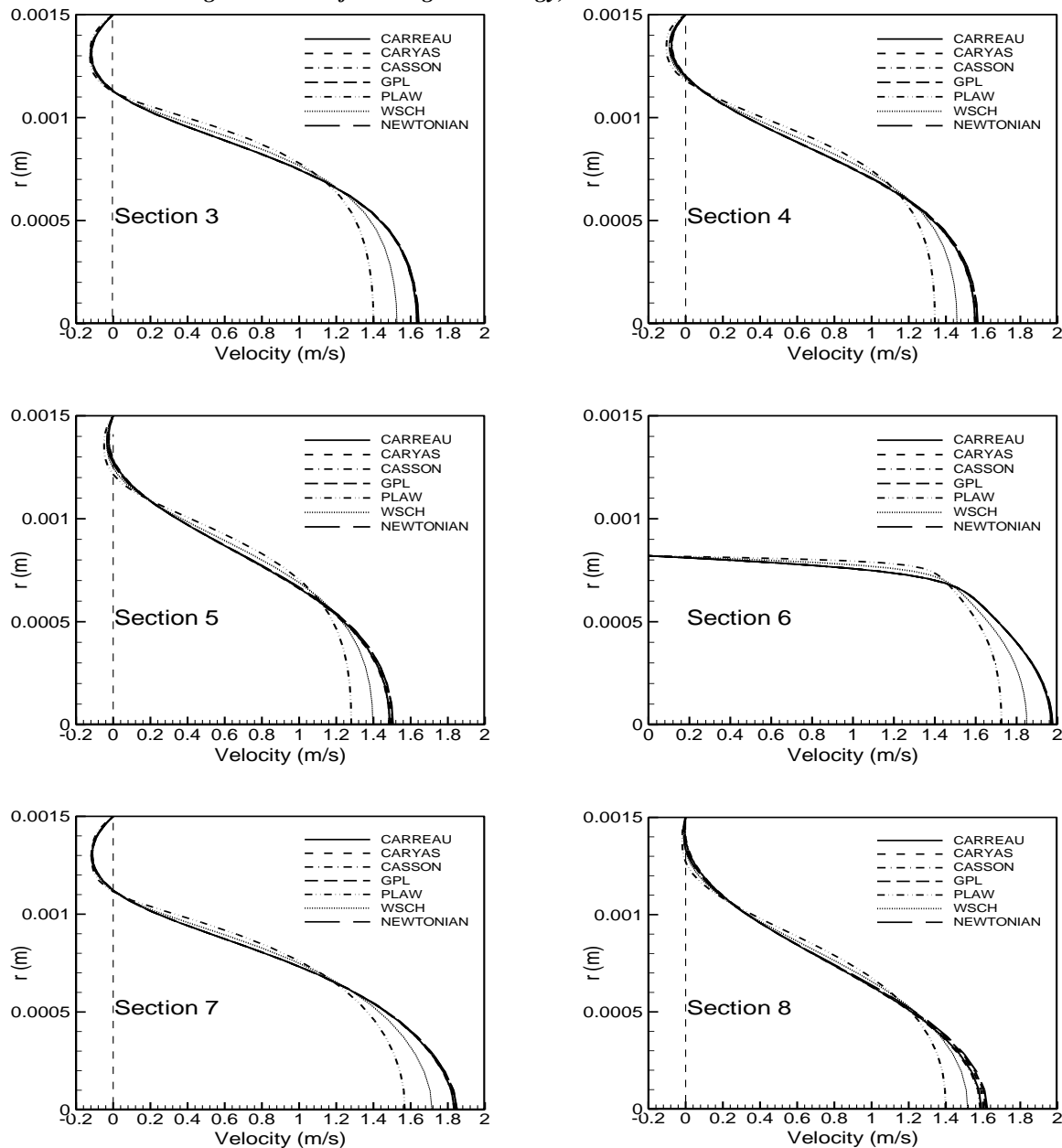


Fig. 5 Axial velocity profile at difference location, 70% stenosis, t=0.24s

Figs. 6 and 7 show the axial velocity diagram obtained for the Casson model and the Newtonian model respectively in artery with 70% stenosis, distances of 2D-8D, and $t = 0.24$ s. Comparison of the axial velocity profiles at all sections after single and Double adjacent stenosis shows that in double stenosis, axial velocity in the central flow region of the artery exceeds that obtained for the case of simple stenosis. Moreover, reverse flow at regions adjacent to the wall is more common in Double stenosis. Figs. 6 and 7 show that the maximum axial velocity is equal for different distances

of stenosis at the first stenosis. However, at the second stenosis, as can be seen in Table 2, this maximum velocity decreases in the Casson, power law, and Walburn-Schenck models as the distance is increased from 2D to 8D but in the Newtonian model as well as the Carreau, Carreau-Yasuda, and generalized Power law models, the maximum axial velocity first decreases as the distance increases from 2D to 3D, and then decreases as the distance further increases from 4D to 8D.

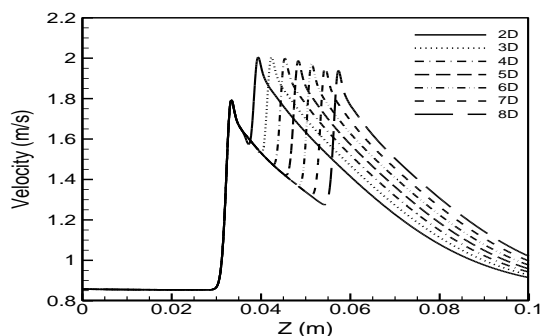


Fig. 6 Axial velocity, Casson, 70% stenosis

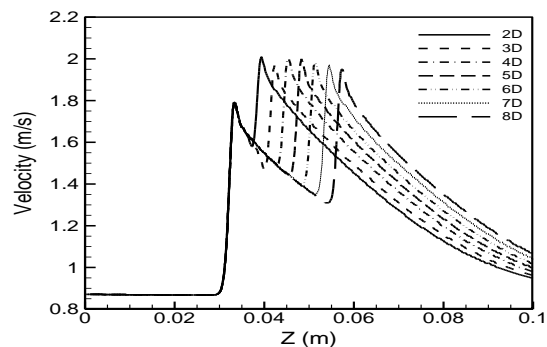


Fig. 7 Axial velocity, Newtonian, 70% stenosis

Table 2 Maximum axial velocity, 70% stenosis, distance between two stenosis=2D up to 8D

Distance between two stenosis	2D	3D	4D	5D	6D	7D	8D
Newtonian	2.01	1.97	2	2	1.98	1.97	1.95
Carreau	2.00336	1.9614	1.9979	1.9872	1.9732	1.9571	1.94
Carreau-Yasuda	2.004	1.9646	2	1.9903	1.9771	1.9617	1.9452
Modified-Casson	2.0053	2.0052	1.999	1.9877	1.973	1.9563	1.9388
Generalized power-law	2.0059	1.9661	2.0033	1.9943	1.9818	1.9668	1.9506
Power-law	1.7445	1.7419	1.7387	1.7347	1.7299	1.7244	1.7182
Walburn-Schneck	1.8709	1.87	1.8684	1.8633	1.8562	1.8475	1.8386

Table 3 Maximum WSS for second stenosis, $t=0.24s$

Distance between two stenosis	2D	3D	4D	5D	6D	7D	8D
Newtonian	83.4042	86.936	85.2324	86.2048	87.0928	87.8729	88.5462
Carreau	84.2	87.8	86.1581	87.1644	88.067	88.8508	89.5
Carreau-Yasuda	83.6783	87.3032	85.5529	86.539	87.432	88.2126	88.8841
Modified-Casson	84.8826	85.7959	86.8664	87.8907	88.8039	89.5928	90.2643
Generalized power-law	83.4011	86.9318	85.2	86.2009	87.0877	87.8674	88.5405
Power-law	29.3913	29.5136	29.6	29.7862	29.9335	30.0769	30.2114
Walburn-Schneck	52.904	53.2638	53.7	54.0926	54.5094	54.8943	55.2404

If first and second stenosis are closer together, the fewer walls shear stress is exerted on the second stenosis. Table 3 shows maximum value of shear stress on the second stenosis for the studied models in double stenosis located between 2D and 8D apart and at time of $t = 0.24$ s. Figures 8 and 9 show stress distributions shear for the Casson and Newtonian models respectively at 70% stenosis and various distances.

Maximum shear stress at the first stenosis is equal for all models, but at the second stenosis, it varies according to the distance between stenosis. As already mentioned, the first stenosis directs the flow towards the axis of the artery, leading to a reduction in shear stress at the second stenosis. As the distance between stenosis decreases, the flow would not have sufficient time to immediately spread along the artery wall. Therefore, less shear stress has been observed at the second stenosis. In the Casson, power law, and Walburn-Schneck models, axial velocity decreases as distance increases from 2D to 8D. Moreover, as the flow rate is constant, the velocity gradient at the wall increases as the distance increases

from 2D to 8D. Therefore, as the distance increases, all the mentioned models show an increase in their shear stress at the wall (Fig. 8).

In the Newtonian, Carreau, Carreau-Yasuda, and generalized power law; although the maximum velocity, and consequently the shear stress, does not follow a constant trend as the distance increases from 2D to 8D, in these models, maximum axial velocity decreases with the increase in distance from 2D to 3D, and, therefore, velocity gradient also increases with increasing distance from 2D to 3D, leading to an increase in shear stress. In the 3D to 4D range, axial velocity in these models increases and therefore velocity gradient and shearing stress decrease. In the 4D up to 8D range, axial velocity decreases and, ultimately, shear stress increases. Fig. 10 shows the maximum shear stress values at the first and second stenosis in the Casson model for $t=0.24$ s. The value 0.006 on the horizontal axis indicates two adjacent Double stenosis, and the value 0.024 shows two double stenosis with a distance of 8D between their throats.

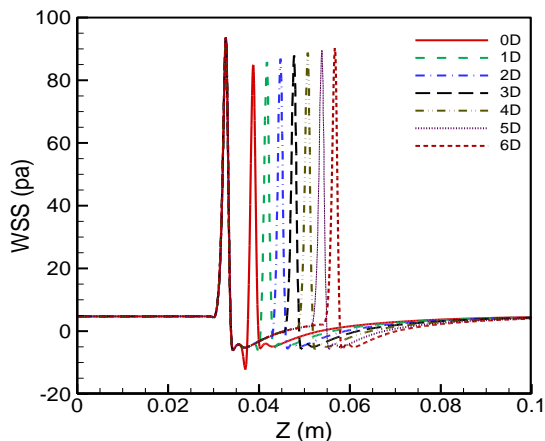


Fig. 8 WSS for Casson model, t=0.24s

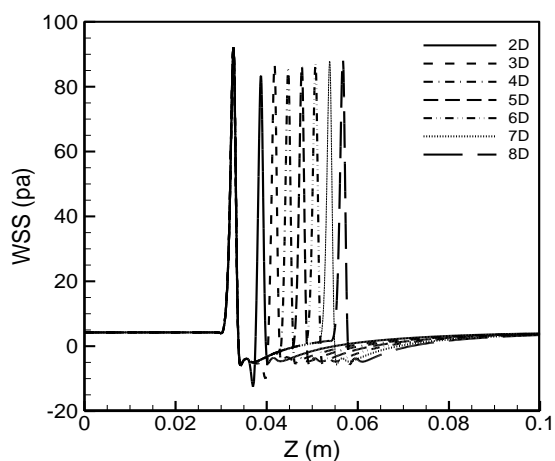


Fig. 9 WSS for Newtonian model, t=0.24s

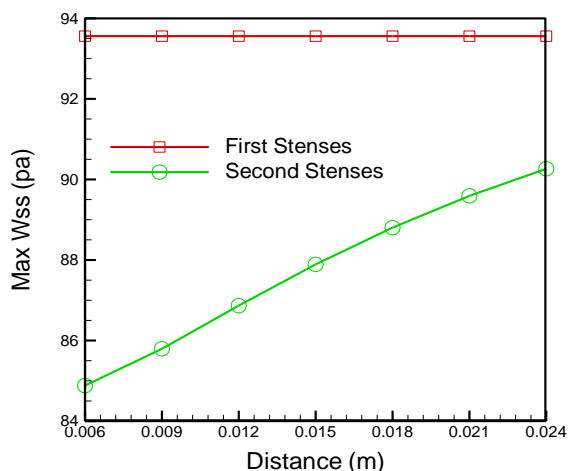


Fig. 10 Trend of Maximum WSS for first and second stenosis, Casson model, t=0.24

5 CONCLUSION

In this paper, we studied an ADINA-aided numerical investigation on the effects of different non-Newtonian models as well as the distance between the stenosis on such parameters as velocity and shear stress. The obtained results showed that maximum shearing stress at the first stenosis is equal for all the models, whereas at the second stenosis, it depends on the distance between the stenosis. The reason is that the first stenosis would divert blood flow towards the blood artery centerline, leading to a reduction in shear stress at the second stenosis. The results obtained for shearing stress profile show that in 70% stenosis, there is the possibility of damage to endothelial cells. Examination of the axial velocity parameter reveals that maximum axial velocity at the first stenosis is the same for all distances. However, at the second stenosis, this velocity decreases for 2D up to 8D range in the Casson, power law, and Walburn-Schneck models. In the Newtonian, Carreau, Carreau-Yasuda, and generalized power law, however, maximum axial velocity decreases in the 2D up to 3D range, increases in the 3D up to 4D range, and once again decreases as the distance between stenosis increases from 4D up to 8D. Another result obtained from comparing various non-Newtonian models is that the values of maximum wall shear stress and maximum axial velocity predicted by power law and Walburn-Schneck models are lower than other non-Newtonian models. Therefore, more caution must be considered when predicting disease is based on these two models.

6 NOMENCLATURE

e	Velocity strain tensor [1/s]
P	Fluid pressure [Pa]
V	Velocity vector [m/s]
F_B	Body force per unit volume [N/m ³]
L_{st}	Length of stenosis region [m]
$R(z)$	Radius of artery in the stenosis region [m]
R_o	Radius of the healthy artery [m]
$R_{o,s}$	Radius of artery at the stenosis throat [m]
z	Axis coordinates of stenosis [m]
z_m	Axis coordinates of stenosis throat from the origin of coordinates [m]
t	Time [s]
ρ	Density [kg/m ³]
μ	Fluid viscosity [kg/m-s]
$\bar{\tau}$	fluid stress tensor [Pa]
$\dot{\gamma}$	Shear rate [1/s]

ACKNOWLEDGMENTS

The authors would like to thank the Islamic Azad University, Shahrekord branch for their supports.

REFERENCES

- [1] Stoltz, J. F., "Hemorheology: Pathophysiological Significance", *Acta Medica Portuguesa*, Vol. 6, No. 7, 1985, pp. 4-13.
- [2] Ishikawa, T., Guimaraes, L. F. R., Oshima, S., and Yamane, R., "Effect of Non-Newtonian Property of Blood on Flow Through a Stenosed Tube", *Fluid Dynamics Research*, Vol. 22, No. 5, 1998, pp. 251-264.
- [3] Mandal, M. S., Mukhopadhyay, S., and Layek, G. C., "Pulsatile Flow of Shear Dependent Fluid in a Stenosed Artery", *Theoretical and Applied Mechanics*, Vol. 39, No. 3, 2012, pp. 209-231.
- [4] Huang, C., Chai, Z., and Shi, B., "Non-Newtonian Effect on Hemodynamic Characteristics of Blood Flow in Stented Cerebral Aneurysm", *Communications in Computational Physics*, Vol. 13, No. 3, 2013, pp. 916-928.
- [5] Rabby, M. G., Shupti, S. P., and Molla, M., "Pulsatile Non-Newtonian Laminar Blood Flows through Arterial Double Stenoses," *Journal of Fluids*, Vol. 1, No. 1, 2014, Article ID 757902, 13 pages.
- [6] Apostolidis, A. J., Moyer, A. P. and Beris, A. N., "Non-Newtonian Effects in Simulations of Coronary Arterial Blood Flow", *Journal of Non-Newtonian Fluid Mechanics*, Vol. 233, No. 1, 2016, pp. 155-165.
- [7] Soares, A. A., Gonzaga, S., Oliveira, C., Simões, A., and Rouboa, A. I., "Computational Fluid Dynamics in Abdominal Aorta Bifurcation: Non-Newtonian Versus Newtonian Blood Flow in a Real Case Study", *Computer Methods in Biomechanics and Biomedical Engineering*, Vol. 20, No. 8, 2017, pp. 1-10.
- [8] Jahangiri, M., Saghafian, M., Sadeghi, and M. R., "Effects of Non-Newtonian Behavior of Blood on Wall Shear Stress in an Elastic Vessel with Simple and Consecutive Stenosis", *Biomedical and Pharmacological Journal*, Vol. 8, No. 1, 2015, pp. 123-131.
- [9] Jahangiri, M., Saghafian, M., and Sadeghi, M. R., "Numerical Simulation of Non-Newtonian Models Effect on Hemodynamic Factors of Pulsatile Blood Flow in Elastic Stenosed Artery", *Journal of Mechanical Science and Technology*, Vol. 31, No. 2, 2017, pp. 1003-1013.
- [10] Fry, D. L., "Acute Vascular Endothelial Changes Associated with Increased Blood Velocity Gradients", *Circulation Research*, Vol. 22, No. 2, 1968, pp. 165-197.
- [11] Ramstack, J. M., Zuckerman, L., and Mockros, L. F., "Shear Induced Activation of Platelets". *Journal of Biomechanics*, Vol. 12, No. 2, 1979, pp. 113-125.
- [12] Fazli, S., Shirani, E., and Sadeghi, M. R., "Numerical Simulation of LDL Mass Transfer in a Common Carotid Artery under Pulsatile Flow", *Journal of Biomechanic*, Vol. 44, No. 1, 2011, pp. 2021-2030.
- [13] Jahangiri, M., Saghafian, M., and Sadeghi, M. R., "Numerical Study of Turbulent Pulsatile Blood Flow Through Stenosed Artery Using Fluid-Solid Interaction", *Computational and Mathematical Methods in Medicine*, Vol. 1, No. 1, 2015, Article ID 515613.
- [14] Jahangiri, M., Saghafian, M., and Sadeghi, M. R., "Numerical Simulation of Hemodynamic Parameters of Turbulent and Pulsatile Blood Flow in Flexible Artery with Single and Double Stenosis", *Journal of Mechanical Science and Technology*, Vol. 29, No. 8, 2015, pp. 3549-3560.
- [15] Jahangiri, M., Saghafian, M., and Sadeghi, M. R., "Numerical Study of Hemodynamic Parameters in Pulsatile Turbulent Blood flow in Flexible Artery with Stenosis", *The 22st Annual International Conference on Mechanical Engineering-ISME2014*, Shahid Chamran University, Ahvaz, Iran, 2014.
- [16] *Theory and Modeling Guide, Volume III: ADINA CFD & FSI, Help of ADINA software*, 2011, pp. 50-60.
- [17] Cho, Y. I., Kensey, K. R., "Effects of Non-Newtonian Viscosity of Blood on Flows in a Diseased Arterial Vessel, Part 1: Steady Flows", *Biorheology*, Vol. 28, No. 3, 1991, pp. 241-262.
- [18] Bird, R. B., Armstrong, R. C., and Hassager, O., "Dynamics of Polymer Liquids", 2nd ed., Wiley, New York, 1987, chap. 3.
- [19] Fung, Y. C., "Biomechanics: Mechanical Properties of Living Tissues", 2nd Edition Springer, Berlin, 1993, chap. 2.
- [20] Ballyk, P. D., Steinman, D. A., and Ethier, C. R., "Simulation of Non-Newtonian Blood Flow in an End-To-End Anastomosis", *Biorheology*, Vol. 31, No. 5, 1994, pp. 565- 586.
- [21] Walburn, F. J., Schneck, D. J., "A Constitutive Equation for Whole Human Blood", *Biorheology*, Vol. 13, No. 3, 1976, pp. 201- 210.
- [22] Sadeghi, M. R., Shirani, E., Tafazzoli-Shadpour, M., and Samaee, M., "The Effects of Stenosis Severity on the Hemodynamic Parameters-Assessment of the Correlation Between Stress Phase Angle and Wall Shear stress", *Journal of Biomechanic*, Vol. 44, No. 15, 2011, pp. 2614-2626.
- [23] Zeng, D., Boutsianis, E., Ammann, M., and Boomsma, K., "A Study on the Compliance of a Right Coronary Artery and Its Impact on Wall Shear Stress", *Journal of Biomechanical Engineering*, Vol. 130, No. 4, 2008, pp. 1- 11.
- [24] Sadeghi, M. R., "Numerical Simulation of Blood Flow in Vessels with Arterial Stenosis Considering Fluid Structure Interaction", Ph.D Dissertation, Graduate school of Mechanical engineering, Isfahan University of Technology, Iran, 2013.
- [25] Jeong, W. W., Rhee, K., "Effects of Surface Geometry and Non-Newtonian Viscosity on the Flow Field in Arterial Stenoses", *Journal of Mechanical Science and Technology*, Vol. 23, No. 9, 2009, pp. 2424-2433.